THE NONLINEAR RESPONSE OF A MULTISTORY PRESTRESSED CONCRETE STRUCTURE TO EARTHQUAKE EXCITATION

by R. A. Spencer [I]

SYNOPSIS

The *nonlinear dynamic responses of two reinforced and six prestressed* concrete versions of a twenty story frame structure to a strong earthquake are found, using a step-by-step integration technique. A special model beam is used to represent the concrete members. The effects of different member properties, different amounts of hysteretic damping, and two different viscous damping mechanisms on response and energy dissipation are compared. The prestressed concrete structures have higher lateral displacements and inter-story drifts, but lower ductility requirements, and the comparative results suggest that a prestressed structure of the type analyzed could withstand a strong earthquake.

GLOSSARY

A	Maximum story acceleration.
D_h	Hysteretic energy dissipation.
D_t	Total energy dissipation.
D_v	Total viscous energy dissipation.
D_{vi}	Interfloor viscous energy dissipation.
D_{vm}	Mass proportional viscous energy dissipation.
EI	Flexural rigidity.
F_c	Compressive force at base of exterior columns.
h	Hinge length factor.
k	Hinge stiffness reduction factor.
k_r	Hinge reversal stiffness factor.
L	Member length.

[I] Assistant Professor in Civil Engineering, University of British Columbia, Vancouver, Canada.

ι Loop width factor.

M_b Base overturning moment.

M_c Cracking moment.

M_e End moment.

M_h Hinge moment.

p Member stiffness reduction factor.

p_r Member reversal stiffness factor.

ξ_m Mass proportion viscous damping factor.

ξ_i Interfloor viscous damping factor.

θ_c Hinge cracking rotation.

θ_h Hinge rotation.

μ_h Hinge ductility factor.

μ_m Member ductility factor.

ϕ_e Member end rotation.

INTRODUCTION

If prestressed concrete members are used as seismic resisting elements in tall frame structures, traditional static methods of design may not be suitable, because of the assumption, implicit in them, that the members can dissipate large amounts of energy by yielding. This is true for plain reinforced concrete members (1), but it is not normally the case when the members are prestressed (2). Thus although confidence has been expressed (3) in the ability of certain types of prestressed concrete structure designed by conventional static methods to withstand strong earthquakes, there is a need for further investigation in the case of frame structures. In this paper the nonlinear dynamic responses of two reinforced and six prestressed concrete versions of a basic 20 story frame structure, designed by static load methods and subjected to a strong earthquake, are calculated and compared.

MEMBER MOMENT-ROTATION LOOPS

In order to make a rational, nonlinear, dynamic frame analysis, it is necessary to know the appropriate end moment-end rotation (M_e-ϕ_e) hysteresis loops for the members. For prestressed concrete members the form of these loops is partly dependent on how the members are loaded, and the loops used here (shown in figure 1) are idealized from loops found by applying equal end moments to test members (2) as shown

in figure 3. The moments varied cyclically about a mean of zero at frequencies of 0.5, 1.0 and 2.0 cycles/second, and no significant frequency dependent effects were observed.

For this loading case, the member stiffness, S_1, when the cracks are closed by the prestress, is:

$$S_1 = 6EI/L \qquad (1)$$

where EI is the appropriate flexural rigidity, and L is the loaded length. Each idealized loop can be completely described by S_1 and four other parameters defined as shown in Figure 1: the cracking moment, M_c, the end moment at which opening of the tension cracks causes the stiffness to fall; the stiffness reduction factor, p, the ratio of the stiffness after cracking to S_1; the reversal stiffness factor, p_r, the ratio of the stiffness when the loop is being crossed to S_1; and the loopwidth factor, ℓ, the ratio of the loopwidth, M_ℓ, to M_c.

It is assumed that a load reversal can occur at any value of ϕ_e without changing the value of p_r. If a number of load reversals occur during a brief time interval, loading back and forth along the same reversal path can occur.

The common assumption is made here that reinforced concrete members can yield, and have M_e-ϕ_e loops like those shown in figure 2, with p = 0.05.

MODEL BEAMS

Each frame member is represented by a model beam, which can have M_e-ϕ_e loops like those in either figure 1 or figure 2. For each model beam, a hinge length factor, h, specifies a short hinge length, hL, at each end as shown in figure 4a. All cracking and energy dissipation in the beam is assumed to occur within these hinge lengths, and the central portion of the beam remains elastic, unaffected by either cracking or load reversal. A hinge length, rather than a simple hinge at a point, is chosen so that distress in the hinge, which depends on the hinge length factor ℓ and the value of p, can be estimated. The hinge length factors used in the analysis are based on observed values (1), (2).

The hinge moment, M_h, or moment at the mid-point of the hinge, and the hinge rotation, θ_h, or angular change over the hinge length, are shown in figure 4a. For prestressed concrete members, an M_h-θ_h hysteresis loop like that shown in figure 4b is specified for each hinge length. The loopwidth is $M_{h\ell}$ and the hinge rotation when equal end moments M_c are applied as in figure 3 is θ_c. When the hinge rotation is less than θ_c, the hinge length is assumed to be uncracked, and its flexural rigidity is EI. When the hinge rotation exceeds θ_c, it is assumed that cracking within the hinge length has reduced its rigidity to kEI. A load reversal in the hinge length, indicated by a change in the sign of θ_h, causes the hinge flexural rigidity to rise to k_rEI until the M_h-θ_h loop is crossed. Values

of k and k_r which give the required values of p and p_r for loading like that shown in figure 3 are found for each value of h by applying the area-moment equations to the whole member. In the response analysis, each hinge length is considered independently, and the overall stiffness of the member then depends on the hinge conditions at each end.

The complex behavior of a real hinge, in which high concrete strains and bond slip both contribute to the reduction in stiffness and to the energy dissipation, is represented here by the action of two beams acting in parallel, and joined along their length so that they always have identical deflected shapes. The first beam is always elastic, and cracking in the hinge length is assumed to reduce its flexural rigidity from EI to kEI. The second beam is shown in figure 4c. It is an assembly of series-connected elastic beams of infinitesimal length, separated by friction dampers which rotate whenever their friction moment is exceeded. The flexural rigidity of the series-connected beams is always such that whenever the dampers are not slipping, the combined flexural rigidity of the two parallel beams is $k_r EI$.

The behavior of the beam-damper assembly can be understood by considering what happens when equal end moments are applied to a member as shown in figure 3, to load it for the first time. Initially both of the parallel beams deflect elastically with a combined flexural rigidity of $k_r EI$. When the moment at the mid-point of the beam-damper assembly reaches $M_{h\ell}/2$, all the friction dampers are assumed to start to slip, the effective flexural rigidity of the assembly falls to zero, and the flexural rigidity of the hinge falls to EI or kEI. As loading continues the friction moment at any distance x from the mid-point of the beam-damper assembly, given by the linear function $M_f(x)$ shown in figure 4d, is assumed to remain constant, and the dampers continue to slip until the first load reversal occurs. They then stop slipping, and the assembly again behaves like an elastic beam. The hinge length has stiffness $k_r EI$, and the moment carried by the beam-damper assembly starts to fall. When it reaches $-M_{h\ell}/2$ at the mid-point, all the dampers again begin to slip, with a new variation of the friction moment along the assembly. Thus the beam-damper assembly controls the energy dissipation and the reversal stiffness of the hinge length.

The energy dissipated, ΔD_h, when the hinge rotation changes by $\Delta\theta$, is found by considering each damper. If the linear function giving the change in curvature at some distance x from the mid-point of the hinge is $\Delta\Psi(x)$, then the total energy dissipation for the hinge length is:

$$\Delta D_h = \int_{-hL/2}^{hL/2} M_f(x).\Delta\Psi(x).dx \qquad (2)$$

When ΔD_h is being found for the frame members, $M_f(x)$ and $\Delta\Psi(x)$ are assumed to be linear functions like those shown in figure 4d.

The width, $M_{h\ell}$, of the M_h-θ_h loop, is chosen so that the M_e-ϕ_e loop has the specified width $\ell.M_c$ when the member is loaded as shown in figure 3, and the hinge lengths are cracked when reversal occurs. With the same type of loading, if there is no cracking when the reversal occurs, the width of the M_e-ϕ_e loop will be less than $\ell.M_c$.

To model the M_e-ϕ_e loop for the reinforced concrete member, shown in figure 2, the reversal stiffness factor k_r is taken as 1, and the loop-width, M_ℓ, of the M_e-ϕ_e loop is:

$$M_\ell = 2.M_c(1-p) \tag{3}$$

In the response analysis, the initial loading of a prestressed member is assumed to be along the backbone curve of the M_e-ϕ_e loop, and not along a reversal path as discussed above. The M_h-θ_h loops do not vary during a response analysis, but because each hinge is considered independently, the M_e-ϕ_e loops can differ from those for the ideal loading case described above.

VISCOUS DAMPING

Because complete information is not available about the damping mechanisms in real structures, two viscous damping mechanisms commonly used in structural analysis are assumed, in addition to the hysteretic damping in the members. The first, mass proportional viscous damping, is expressed by:

$$\alpha M\dot{\underline{U}}$$

where α is a scalar constant, M is the 20x20 diagonal mass matrix, and $\dot{\underline{U}}$ is the vector of velocities of the floors relative to the ground. The second mechanism is a form of interfloor viscous damping, expressed by:

$$\beta K\dot{\underline{U}}$$

where β is a scalar constant and K is the tri-diagonal stiffness matrix for the special case when all girders are assumed to be rigid, and the columns are flexible but do not crack. These expressions appear in the linear matrix equation of motion as:

$$M\ddot{\underline{y}} + (\alpha M + \beta K)\dot{\underline{U}} + K'\underline{U} = 0 \tag{4}$$

where $\ddot{\underline{y}}$ is the vector of absolute story accelerations, K' is the 20x20 full stiffness matrix for the real structure with flexible columns and girders, and $\underline{U}$ is the vector of story displacements relative to the ground.

For mass proportional damping only, the fraction of critical damping in the first mode, ξ_m, is given by:

$$\xi_m = \frac{\alpha}{2\omega_1} \tag{5}$$

where ω_1 is the circular natural frequency of the first mode. For true stiffness proportional interfloor viscous damping only, expressed by:

$$\beta' K' \dot{\underline{U}}$$

where β' is a scalar constant, the fraction of critical damping in the first mode is:

$$\xi_i' = \frac{\beta' \omega_1}{2} \tag{6}$$

To find an equivalent fraction of critical damping, ξ_i, for the non-proportional interfloor damping mechanism actually used, the two mechanisms $\beta K \dot{\underline{U}}$ and $\beta' K' \dot{\underline{U}}$ are assumed to be equivalent if both dissipate the same amount of energy per cycle, when the structure is vibrating with frequency ω_1 and displacement vector $\underline{U}_1 \sin(\omega_1 t)$, where $\underline{U}_1$ is the first mode shape for the undamped structure. This requires that:

$$\beta \underline{U}_1^t K \underline{U}_1 = \beta' \underline{U}_1^t K' \underline{U}_1 \tag{7}$$

For the structure analyzed equation (7) gives:

$$\beta' \approx 3.3\beta \tag{8}$$

Using equation (6), ξ_i is found to be:

$$\xi_i = \frac{3.3\beta\omega_1}{2} \tag{9}$$

The choice of an interfloor damping mechanism using K rather than K' was made to reduce computational difficulties.

NONLINEAR EQUATIONS OF MOTION

The nonlinear equations of motion were solved with a computer, using a step-by-step integration technique with finite time increments. The structure was assumed to remain linear throughout any given time increment, so the nonlinear response is the sum of the results of a series of incremental linear analyses. A matrix substitution method (4), (5), was used to solve the linear equations of motion for each time increment. Conditions at every hinge were examined after every time increment, and member properties were varied if necessary before the next increment began. The foundation of the structure was assumed to be rigid, and torsion was neglected. The masses were concentrated at the floor levels and only moved horizontally, and the floors contributed no additional stiffness.

The magnitude of the time increment used was 0.005 seconds, which is approximately one sixth of the period of the 20^{th} mode.

The hysteretic energy, ΔD_h, dissipated by each hinge was found after every incremental analysis. The incremental viscous energy dissipation

at each floor level was found by assuming that a force, equal to the mean of the viscous forces acting at the beginning and end of the increment, acted throughout the interval. Mass proportional and interfloor viscous energy dissipations were found separately.

EXCITATION

The excitation used in each analysis was the first 8 seconds of the accelerogram of the El Centro 1940 earthquake, N-S component. This has a peak acceleration of 0.32g, which occurs 2 seconds after the start of the record, and a peak spectral frequency of 14 rad/sec (6).

STRUCTURE ANALYZED

The basic properties of the structure analyzed are shown in figure 5 and Table 1. It was designed by Clough and Benuska (7), who found the relative stiffnesses of the members by applying dead loads and live loads plus code (8) lateral forces for earthquake. Member flexural rigidities were specified in terms of a reference value, EI_o = 133,500 Kip. ft.^{2} which gave a natural period of 2.2 seconds. An exact computer analysis was then made to find the "design" moments resulting from the static application of the horizontal and vertical design forces. Cracking moments were taken as twice the design moments for the girders, and six times the design moments for the columns. Two reinforced and six prestressed concrete versions of this structure are considered here.

RESULTS PRESENTED

All the results presented, except those for dissipated energy, are maximum values recorded during the eight seconds of earthquake excitation.

As a measure of nonlinear deformation, two different ductility factors were found for each end of every member. The member ductility factor, μ_m, is:

$$\mu_m = \frac{\phi_{max}}{\phi_\ell} \quad (\phi_{max} \geq \phi_c)$$
$$\mu_m = \frac{\phi_{max}}{\phi_c} \quad (\phi_{max} < \phi_c) \qquad (8)$$

where ϕ_{max} is the maximum recorded end rotation, and ϕ_ℓ is found as shown in figure 6, using the M_e-ϕ_e loop for equal end moments applied to the member as shown in figure 3.

The hinge ductility factor, μ_h, is:

$$\mu_h = \frac{\theta_{max}}{\theta_c} \qquad (9)$$

where θ_{max} is the maximum recorded hinge rotation. With the beam model used, μ_m is generally less than μ_h, because the member stiffness reduction factor, p, is greater than the hinge stiffness reduction factor, k. Ductility requirements for structural members are usually given in terms of member ductility factors similar to μ_m, but some test results (1) have been given in terms of hinge ductility factors.

Values of the base overturning moment, M_b, and the compressive force at the base of the exterior column, F_c, result from the moments and shears induced by lateral displacement of the structure, and do not include gravity and dead load effects.

The results given for dissipated energy are all based on cumulative totals for the eight seconds of excitation. Values for the entire structure are: The total energy dissipated, D_t; the ratio of viscous to hysteretic energy dissipation, D_v/D_h; and the ratio of mass proportional to inter-floor viscous energy dissipation, D_{vm}/D_{vi}. Some values of the energy dissipated on each story level are given graphically.

DISCUSSION OF RESULTS

Reinforced Concrete Structures: For comparison with the prestressed structures, two structures with members having M_e-ϕ_e properties as shown in figure 2 were analyzed. Both had p = 0.05 for all members. The hinge length factors were h = 0.05 for the girders, and h = 0.07 for the columns, giving hinge lengths of 12 in. and 10 in. respectively, which are similar to observed values (1). Structure 1 had mass proportional viscous damping only, with $\xi_m = 0.1$. Structure 2 had interfloor viscous damping only, with $\xi_i = 0.05$. Nonlinear response results for structure 1 have been found previously (5), (7).

Figure 7 shows that the mass proportional damping is more effective in controlling lateral displacements, but figures 9, 11 and 13 show that the interfloor damping is more effective in controlling interstory drift, girder member ductility, and girder hinge ductility respectively. Table 2 confirms this for the maximum column ductility factors. The interfloor damping controls nonlinear deformations more effectively because it has a progressively greater effect on the higher modes. Figures 11 and 13 also show the significant difference between the largest values of μ_m (4.3) and μ_h (16.8) for the girders of structure 1. Although the beam model used is a simple one, a similar difference between μ_m and μ_h might be found for real members.

Table 2 shows the effectiveness of the interfloor damping in reducing the maximum absolute story acceleration, A. The value of 0.82g for structure 1, recorded on the 17th floor, is probably high enough to damage non-structural elements and equipment. The value of 0.31g for structure 2, recorded on the first floor, is less than the maximum base acceleration of 0.32g, and appears to be too low to be realistic.

The significance of the values of M_b and F_c given in Table 2 is discussed later.

Figures 14 and 15 show how much energy was dissipated at each floor level by viscous damping and by hysteretic damping, for structures 1 and 2 respectively. Table 2 gives energy dissipation results for the entire structures. It seems clear from these results that neither of the viscous damping mechanisms used accurately model mechanisms likely to operate in real structures. The gradual fall in energy dissipation toward the base with mass proportional damping, and the sharp peaks for certain floors with interfloor damping, both appear to be rather unrealistic. However, the use of these mechanisms when comparing the responses of different structures appears to be justified, until more accurate models of the real mechanisms are available. Because of the simple M_e-ϕ_e diagram used, there is no hysteretic energy dissipation when elastic hinge rotation occurs after some plastic rotation has been incurred by a hinge, so that the relatively large values of D_v/D_h (0.70 and 1.15) are perhaps not unreasonable.

Prestressed Concrete Structures: The basic prestressed structure had the same member flexural rigidities and cracking moments as structures 1 and 2. This is not intended to represent an economical prestressed design — it is used to show the effects of a direct substitution of prestressed for reinforced concrete members. The hinge length factor used for all members, $h = 0.2$, was based on experimentally observed values (2). The reversal stiffness factor was $p_r = 2.0$, to ensure that the M_e-ϕ_e loops were crossed reasonably quickly.

In structure 3 the stiffness reduction and loopwidth factors used were $p = 0.2$ and $\ell = 0.2$ for the girders, and $p = 0.5$ and $\ell = 0.05$ for the columns. These values are based on test results (2). The girder and column values are different because the columns have a higher ratio of cracking to design moment than the girders. This requires a higher prestress in the columns, which increases p and tends to reduce ℓ (by reducing cracking and bond slip). It also results in less post-cracking deformation, which further increases p and reduces ℓ. Mass proportional viscous damping, with $\xi_m = 0.1$, was used.

The lateral story displacements shown in figure 7 are all larger than the corresponding values for structure 1, which had similar viscous damping. The interstory drifts shown in figure 9 are also generally greater than those of structure 1, although the maximum drift recorded for structure 3 (1.1 in.) is less than that for structure 1 (1.29 in.). Values of μ_m for the girders, shown in figure 11, have a maximum of 2.6, and

Table 2 shows the maximum column value is only 1.7. These values show that although the interfloor deflections might be large enough to cause non-structural damage, no structural damage to the members should occur, since member ductility factors of at least four are possible, without structural damage, for properly designed prestressed members.

Figure 13 shows that the maximum value of μ_h for the girders is 5.4, compared with 16.8 for structure 1. This difference is partly due to the greater hinge length assumed for the prestressed members. The simple beam model used gives no indication of how the curvature is distributed within the hinge length, but prestressing does delay the development of curvature concentrations due to steel yielding, so these values of μ_h should give an indication of the relative amounts of concrete distress to be expected within prestressed and reinforced concrete hinges.

Table 2 shows that the maximum story acceleration, A, is only slightly higher than for structure 1, but the values of M_b and F_c are much higher. These are discussed later.

The ratio $D_v/D_f = 2.28$ in Table 2 is higher than that for structure 1, and suggests that too much viscous damping has been included.

In structure 4, the viscous damping was changed to interfloor damping, with $\xi_i = 0.05$. The other parameters were the same as for structure 3. The lateral displacements shown in figure 7 are all larger than those for structure 3 and the interstory drifts shown in figure 9 are generally larger. Figure 11 and Table 2 show ductility factors which reflect these changes. The values of A in Table 2 show that interfloor damping reduced the absolute story accelerations, just as it did for structure 2.

The ratio of $D_v/D_f = 2.82$ was higher than that for structure 3, although the viscous damping factor was less. This value suggests that as in structure 3, viscous damping is responsible for too much of the total energy dissipation. The sharply peaked curve for D_v in figure 16 suggests that this is in part the result of the high relative interstory velocities associated with the higher modes. This confirms that until more information is available about damping mechanisms, these results should only be used for comparative purposes.

In structure 5, both types of viscous damping were included, with $\xi_m = 0.01$ and $\xi_i = 0.02$. Figures 8 and 10 show that the lateral displacements and the interstory drifts all exceeded those of structures 3 and 4. Ductility factors were also correspondingly large, but as seen from figure 12 and Table 2, did not indicate excessively large nonlinear member deformations.

Table 2 shows that the base overturning moment, $M_b = 89 \times 10^3$ Kip. ft., and the external column compressive force, $F_c = 1376$ Kips., were also the highest recorded. The dead load contribution to M_b found by simultaneously giving each story its maximum lateral displacement was only 4.3×10^3 Kip. ft., or about 5% of M_b, so from this point of view the

lateral displacements are apparently not excessive. Since the static moment required for overturning is 154 x 10^3 Kip. ft., it is the axial column load at the base which is more significant.

For each structure the static dead load produces a compressive force in the outer columns of 860 Kips. The application of the code (9) lateral loads for earthquake, (with no reduction factor for overturning moment) adds only another 335 Kips., whereas Table 2 shows that F_c, the maximum value of the added compressive force due to dynamic loading, varied from 847 Kip. for structure 1 to 1376 Kips. for structure 5. Thus static design methods give a very low estimate of column compressive forces.

The dissipated energy values in Table 2 show that reducing the amount of viscous damping has only reduced D_v/D_h to 1.91. The ratio of $D_{vm}/D_{vi} = 0.22$ shows the much greater effectiveness of the interfloor damping in dissipating energy.

For structure 6 it was assumed that some of the energy dissipated by walls, floors, partitions, etc., could be included in the M_e-ϕ_e loops. Loopwidth factors were doubled, giving $\ell = 0.4$ for the girders and $\ell = 0.1$ for the columns. Viscous damping was the same as for structure 5, with $\xi_m = 0.01$ and $\xi_i = 0.02$. Figures 8, 10 and 12 and Table 2 show that the increased hysteretic damping was effective in reducing the response. The ratio $D_v/D_h = 0.91$, and a total energy dissipation, D_t, only slightly higher than for structure 5, suggest that as more hysteretic energy dissipation is assumed, the viscous damping becomes more acceptable.

In structure 7, the stiffness reduction factors were halved, giving $p = 0.1$ for the girders and $p = 0.25$ for the columns. Viscous damping and loopwidths were the same as for structure 6, and the results given in figures 8, 10, and 12, and in Table 2, should be compared with the results for that structure. A small increase in displacements and deformations, and a decrease in M_b and F_c, can be seen, so that changing p does not appear to significantly affect the response.

Structure 8 represents a more practical prestressed design, in which column cracking moments are reduced to only twice the design moments. This would allow a prestress of about 1000 psi in typical members, assuming an elastic modulus for concrete of $3 \cdot 10^6$ psi for this type of loading (2). Factors of $p = 0.2$, (suggested by test results (2)) and $\ell = 0.4$ (as for structure 6), were used for all members. Viscous damping was included, with $\xi_m = 0.01$ and $\xi_i = 0.02$. Figure 17 shows the energy dissipated on each floor. The reduction in the peak values of the interfloor viscous energy dissipation compared with structures 2 and 4 is very marked, and the combination of viscous and hysteretic damping used in structure 8 appears to be reasonable. A comparison of the results in figures 8, 10, 12 and 17, and in Table 2, with those for the other structures, including the two reinforced structures, suggests that if allowance is made for relatively high interstory drifts and compressive forces in the columns, structure 8 would represent a satisfactory design to withstand the earthquake excitation used.

CONCLUSION

From this comparative study it appears that a prestressed concrete structure could be designed to withstand a strong earthquake. There would be no structural damage to the prestressed concrete members, but non-structural damage as a result of excessive interstory drift might be more widespread than with a reinforced concrete frame. Large compressive forces in the exterior columns would have to be allowed for.

Efforts to control response by increasing hysteretic energy dissipation would be well worthwhile, but there is little to be gained by increasing p.

Because the damping mechanisms are not well enough understood, analyses of this kind should at present be used to make comparative studies, involving some structures which are known to be satisfactory for earthquake loading.

ACKNOWLEDGEMENTS

This study was supported by a grant from the National Science Foundation. Some of the computer programs used are similar to programs developed and written by M. F. Giberson.

BIBLIOGRAPHY

(1) Hanson, N. W. and Connor, H. W., "Seismic Resistance of Reinforced Concrete Beam-Column Joints," Proc. ASCE, Vol. 93, No. ST5, October 1967.
(2) Spencer, R. A., "Stiffness and Damping of Cyclically Loaded Prestressed Members," Presented at the 2nd Mexican Congress on Earthquake Engineering, Vera Cruz, May 1968.
(3) Lin, T. Y., "The Design of Prestressed Concrete Buildings for Earthquake Resistance, : Proc. ASCE, Vol. 91, No. ST5, October 1965.
(4) Clough, R. W., King, I. P., and Wilson, E. L., "Large Capacity Multistory Frame Analysis Programs," Proc. ASCE, Vol. 89, No. ST4, August 1963.
(5) Giberson, M. F., "The Response of Nonlinear Multi-Story Structures Subjected to Earthquake Exitation," Ph.D. thesis, California Institute of Technology, May 1967.
(6) Jenschke, V. A., Clough, R. W. and Penzien, J., "Characteristics of Strong Ground Motion, "Proc. 3rd World Conf. on Earthquake Engineering, New Zealand, 1965.
(7) Clough, R. W. and Benuska, K. L., "Nonlinear Earthquake Behavior of Tall Buildings," Proc. ASCE, Vol. 93, No. EM3, June 1967.
(8) "Uniform Building Code," Int. Conf. of Building Officials, Calif., 1964.
(9) "Uniform Building Code," Int. Conf. of Building Officials, Calif., 1967.

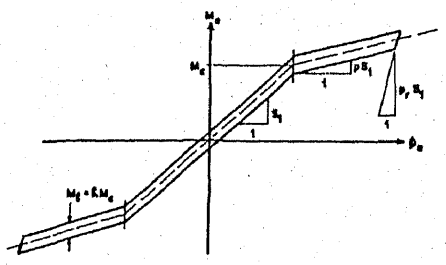

Figure 1: Typical M_c-ϕ_c hysteresis loop for prestressed concrete members.

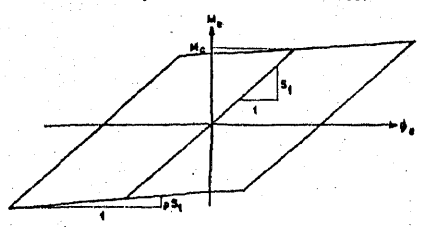

Figure 2: Typical M_c-ϕ_c hysteresis loop for reinforced concrete members.

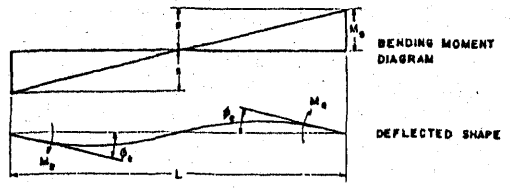

Figure 3: Loading applied to test members

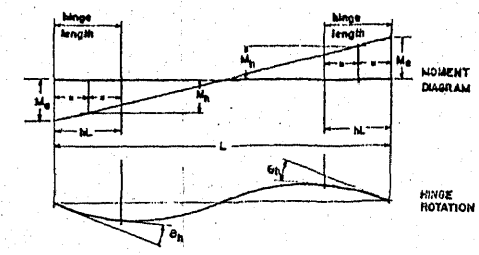

Figure 4a: M_h and θ_h defined for a hinge length

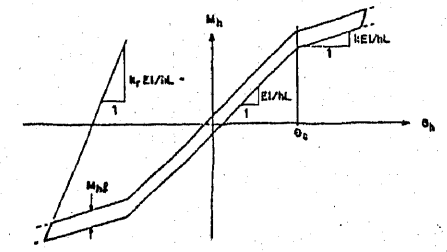

Figure 4b: Typical M_h-θ_h hysteresis loop for a prestressed hinge length

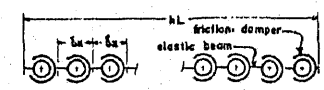

Figure 4c: Series connected beam-damper assembly.

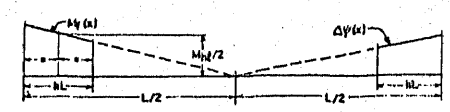

Figure 4d: Functions $M_f(x)$ and $\Delta\psi(x)$

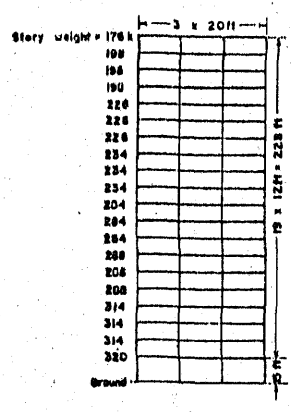

Figure 5: Properties of structure.

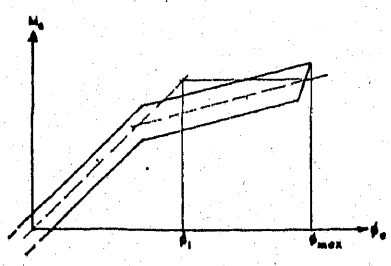

Figure 6: Definition of ϕ_{max} and ϕ_1 for member ductility factor.

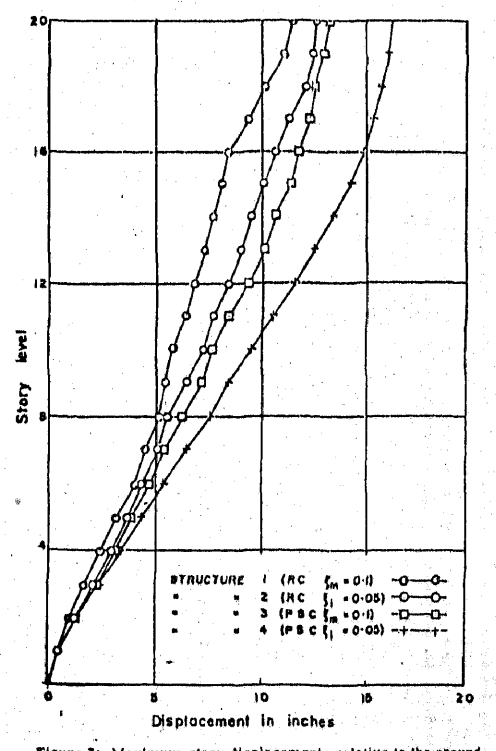

Figure 7: Maximum story displacements relative to the ground.

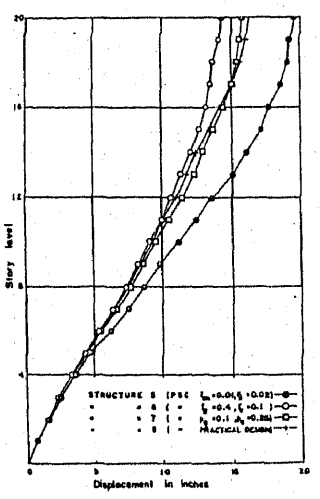

Figure 8: Maximum story displacements relative to the ground.

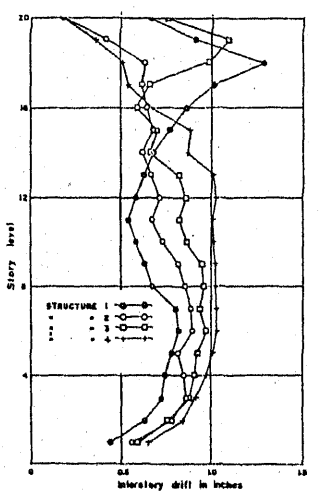

Figure 9: Maximum interstory drifts.

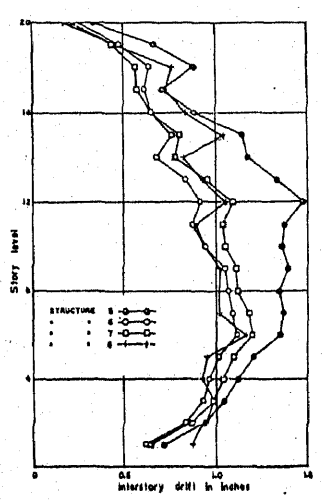

Figure 10: Maximum interstory drifts.

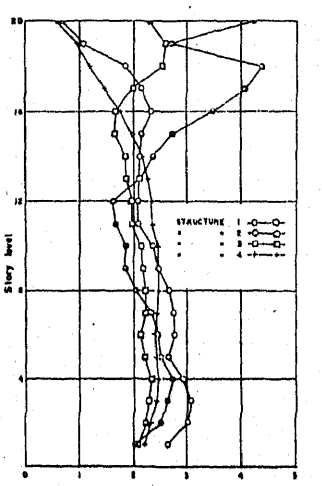

Figure 11: Maximum member ductility factors for the girders

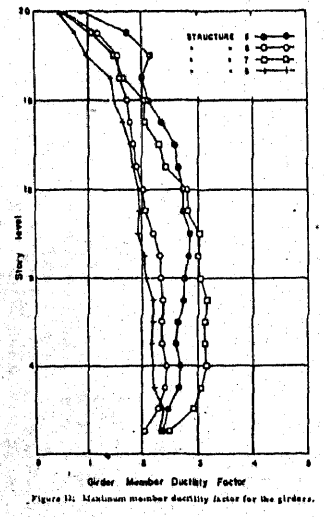

Figure 12: Maximum member ductility factors for the girders.

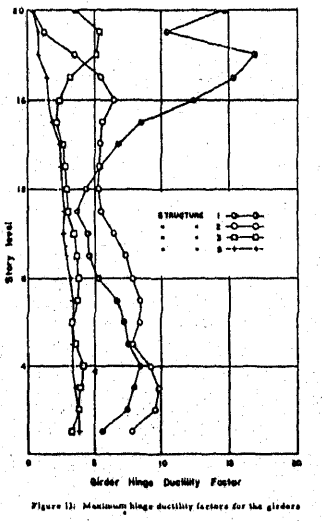

Figure 13: Maximum hinge ductility factors for the girders

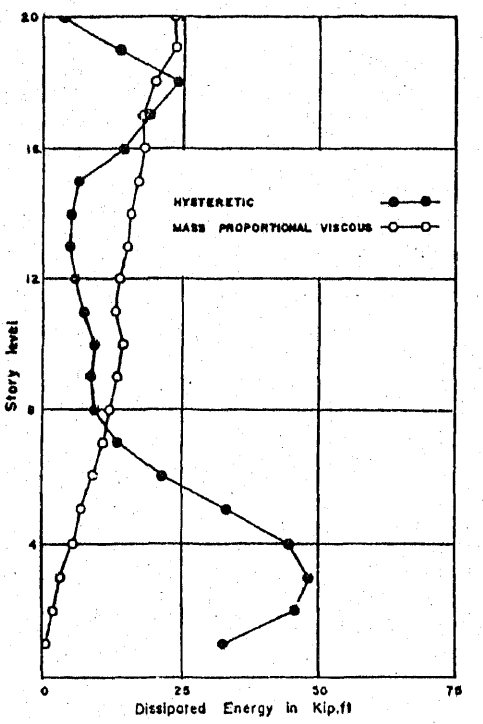

Figure 14: Structure 1: Energy dissipated at each story.

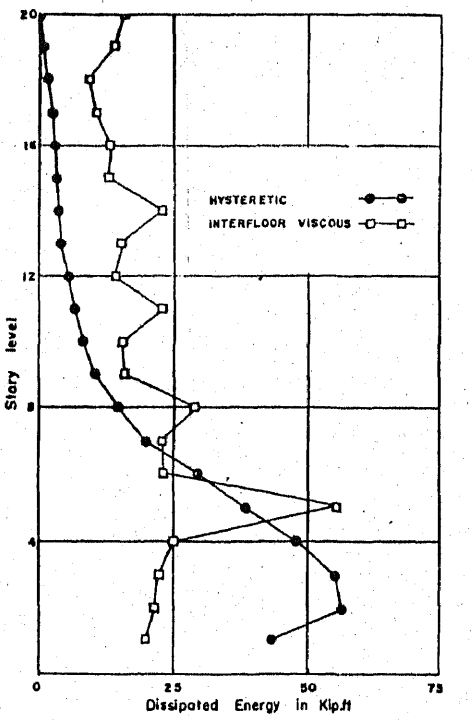

Figure 15: Structure 2: Energy dissipated at each story.

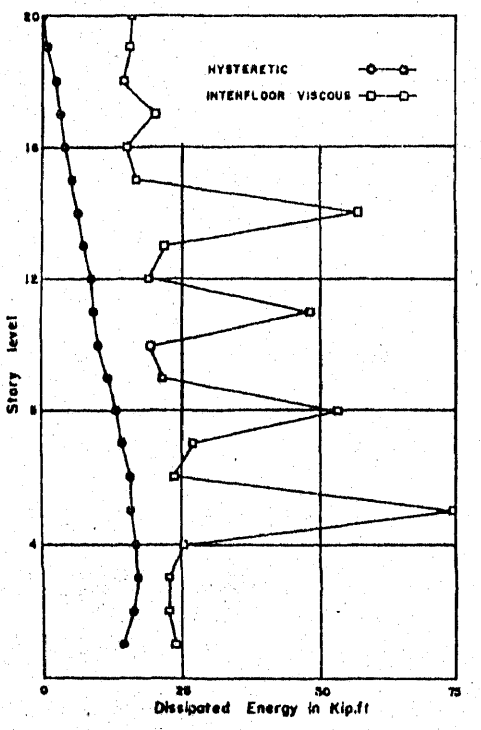

Figure 16: Structure 4: Energy dissipated at each story.

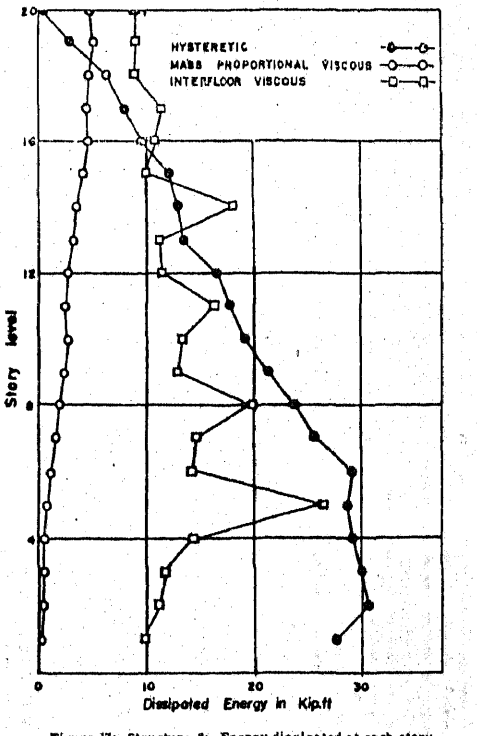

Figure 17: Structure 8: Energy dissipated at each story.

Table 1: Relative Flexural Rigidities of Members

Story levels	EI/EI_o		
	Columns		Girders
	Exterior	Interior	
20-18	1.0	2.0	4.0
17-15	1.5	3.0	6.0
14-12	3.0	6.0	8.0
11-9	4.5	9.0	
8-6	6.0	12.0	
5-3	10.0	20.0	10.0
2-1	12.0	24.0	

Table 2: Maximum Values of Response Parameters

Struc. No.	Col. Ductility		A (frac. g)	M_b (Kip. ft. x 10^3)	F_c (Kips)	D_{vm}/D_{vi}	D_v/D_h	D_t (Kip. ft.)
	Member	Hinge						
1	2.9 [1] (20)	7.2 [1] (20)	0.82 [1] (17)	55	847	–	0.70	626
2	0.8 (1)	0.8 (1)	0.31 (1)	59	916	–	1.15	752
3	1.7 (20)	3.0 (20)	0.84 (16)	74	1150	–	2.28	684
4	1.0 (1)	1.0 (1)	0.31 (1)	83	1288	–	2.82	764
5	1.9 (1)	1.1 (1)	0.43 (20)	89	1376	0.22	1.91	704
6	0.9 (1)	0.9 (1)	0.41 (20)	85	1314	0.20	0.91	705
7	0.9 (1)	0.9 (1)	0.36 (20)	78	1196	0.20	0.92	706
8	3.7 (1)	6.3 (1)	0.34 (20)	78	1233	0.22	0.85	691

[1] Story level where this value was recorded.